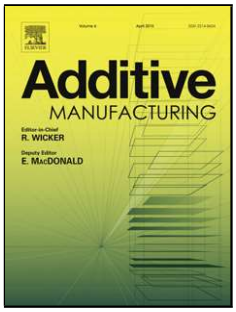

Title: New scanning strategy to reduce warpage in additive manufacturing

Authors: Davi Leão Ramos, Fawzi Belblidia, Johann Sienz

PII: S2214-8604(18)30552-9
DOI: https://doi.org/10.1016/j.addma.2019.05.016
Reference: ADDMA 730

To appear in:

Received date: 4 February 2019
Revised date: 24 April 2019
Accepted date: 14 May 2019

Please cite this article as: Ramos DL, Belblidia F, Sienz J, New scanning strategy to reduce warpage in additive manufacturing, *Additive Manufacturing* (2019), https://doi.org/10.1016/j.addma.2019.05.016

New scanning strategy to reduce warpage in additive manufacturing

Davi Leão Ramos, first author[1]

College of Engineering, Swansea University

Fabian Way, Crymlyn Burrows, Skewen, Swansea SA1 8EN

805292@swansea.ac.uk

Fawzi Belblidia, second author

College of Engineering, Swansea University

Fabian Way, Crymlyn Burrows, Skewen, Swansea SA1 8EN

f.belblidia@swansea.ac.uk

Johann Sienz, third author

College of Engineering, Swansea University

Fabian Way, Crymlyn Burrows, Skewen, Swansea SA1 8EN

j.sienz@swansea.ac.uk

Abstract

This paper proposes a novel geometric based scanning strategy adopted in the selective laser melting (SLM) manufacturing technology aimed at reducing the level of residual stresses generated during the build-up process. A set of computer simulations of the build, based on different scans strategies, including temperature dependent material properties, and a moving heat flux, were performed. The research novelty explores intermittent scan strategies in order to analyze the effect of reduction on heat concentration on the residual stress and deformation. Coupled thermal-structural computations revealed a significant stress and warpage reduction on the proposed scanning scheme. Different powder material properties were investigated and the computational model was validated against published numerical and experimental studies.

NOMENCLATURE

ρ	density
C_p	specific heat capacity
T	temperature
$\boldsymbol{q}$	heat flux
Q	rate of heat per unit of volume
H	velocity
H	Enthalpy
k	thermal conductivity
T_0	ambient temperature
Γ	whole domain
Γ_q	boundary where the laser heat flux is applied
$\vec{n}$	unit normal vector
q_{conv}	heat loss through convection
h	film convection coefficient of the domain
T_S	temperature on the surface
Γ_{conv}	boundary where convection is applied
$\boldsymbol{\sigma}$	Cauchy stress tensor
$\boldsymbol{b}$	body force
$\boldsymbol{C}$	stress-strain matrix
$\boldsymbol{\epsilon}$	total strain

$\boldsymbol{\epsilon}^e$	elastic strain
$\boldsymbol{\epsilon}^p$	plastic strain
$\boldsymbol{\epsilon}^T$	thermal strain
α	coefficient of thermal expansion
T_{ref}	reference temperature
$\boldsymbol{I}$	identity matrix
f	yield function
σ_m	Mises' stress
σ_y	yield stress
$d\boldsymbol{\epsilon}^p$	plastic strain increment
$d\boldsymbol{\lambda}$	plastic multiplier
Q_G	heat flux of Gaussian model
A	absorptance
P	laser power
R	laser spot radius
r	distance to the laser beam centre
B	shape factor
a, b, c	ellipse shape parameters
f^j	value assigned to each j island
α_1, α_2	weighting factors

d_1^j distances between the candidate islands and previous island

d_2^j distances between the current scanned island and previous island

1. Introduction

Additive Manufacturing (AM) refers to the class of manufacturing processes that create three-dimensional components by generating continuous thin slices. The layer creation can be built by a variety of methods such as Direct Energy Deposition (DED), Electron Beam Melting (EBM) and Selective Laser Melting (SLM). In contrast to the traditional manufacturing technologies, SLM has gained a substantial interest in many industries, in particular, aerospace, automotive and biomedical. Furthermore, the design of geometrically unconventional structures allowed the inclusion of advanced techniques, such as topology optimization developed by (Langelaar, 2016), to reduce the material wastage whilst improving the part mechanical performance.

SLM belongs to the family of powder bed fusion technologies, which builds metal parts through a consecutive addition of thin metal powder layers. A laser heats the powder bed melting the track and agglutinating the current layer to the previous one. As the layer is completed the powder bed is lowered, creating space for a new layer to be spread on top of the previous one. Iteratively, the laser heats the material surface following a pre-designated path creating the component cross section, layer by layer, until the part is completely built.

At the location where the laser beam melts the powder, a large temperature gradient is generated leading to the formation of a localised melt-pool in the powder bed. As the laser moves, the instantaneous heating and cooling down of this region leads to the expansion of the heated layer, which is restricted by the underlying material. This induces compressive elastic strains on the solidified layer that can eventually exceed the material's yield strength forming a plastically compressed top layer. As the build is completed, the plastic compression remains embedded within the part and the upper layers start shrinking and warping. This phenomenon, described by Mercelis and Kruth (2006) as temperature gradient mechanism, is

responsible for the residual stresses that might compromise the quality of the finished part.

Predictive models of the residual stresses allow the development of a better and comprehensive part design. An analytical two dimensional beam theory model was introduced by Mercelis and Kruth (2006) to unveil the influence of the base plate height on the level of the residual stress of the part. They concluded that the stress was shown to increase with the base plate height. Alternatively, numerical models based on finite element method (FEM) have been adopted for calculating SLM residual stresses. A two-dimensional linear elastic constitutive model was adopted by Matsumoto et al. (2002) to calculate the residual stresses of a single layer assuming very low Young's modulus to represent the molten part and the powder bed. Hussein et al. (2013a) considered a three-dimensional FEM simulation to compute the temperature and stress fields in a single 316L stainless steel powder bed without underlying solid material. They found that as the laser speed increased, the width and the depth of the melt-pool decreased whilst its length increased.

Other work compared the outcome from different material and process parameters. Particularly, Denlinger et al. (2015) performed both experimental and numerical approaches using titanium and nickel alloys to measure the deformation and residual stress as a function of the cooling time between the completion of the current layer and the beginning of the next. Likewise, Wits et al. (2016) studied the effects of a single vector scanning in order to determine the temperature distribution and molten pool for different values of applied energy density. In their research, experimental and numerical analyses were performed and contrasted to investigate the influence of several sets of process parameters applied during build-up of components. In another study, Zhao et al. (2017) developed a three-dimensional numerical model to study the size of the melt pool and residual stress in a single layer setting. They made a comparison between a uniform and semi-spherical heat flux distribution, predicting a slightly deeper but narrower melt pool for the semi-spherical model.

For the computational modelling, in addition to the different material properties for the powder material, another applied technique known as the "birth and death" method was adopted. The technique mimics the layer per layer build-up

on a fixed initial mesh of the component by activating the elemental stiffness matrix of elements as they are scanned and deactivating before the simulation starts - see Section 2.2 below.

Fu and Guo (2014) applied the birth and death method along with different powder and bulk material properties to determine the temperature history and melt pool shape and size of a multilayer SLM, validated by experiment. Likewise, Foroozmehr et al. (2016) quantified the influence of the laser speed on the melt-pool shape on a multi-track, showing that the melt-pool varied from the beginning of a track to its end reaching a constant size after the third track.

Along with process parameters, the scanning pattern has emerged as an influent mechanism related to the stress build-up. A study by Fox et al. (2011) demonstrated how the build-up process parameter affected the relative density of the build as well as the build time and manufacturing cost. Likewise, Kruth et al. (2004) had found that the residual stress parallel to the scan vector increased with the scan vector length. Their experimental results displayed a smaller deformation along the horizontal and vertical direction when compared against conventional unidirectional scanning strategy. Foroozmehr and Kovacevic (2010) investigated the influence of four types of laser pattern on the residual stress, showing the effect on the temperature history varied significantly, and consequently, the residual stress. In another study conducted by Ma and Bin (2007), two scanning pattern were investigated on a 32 mm square area of a nickel part. The outcome indicated that the residual stress and distortion were reduced with a fractural scanning pattern when compared to the 'S' scan pattern. Similarly, Parry et al. (2016) used three geometries of different sizes and two scan patterns to found that the residual stress increased with scan vector length, and interestingly no substantial difference was detected between the applied laser scan strategies. Likewise, Cheng et al. (2016) conducted a three-dimensional thermo-mechanical simulation to study the effect of 8 different scan strategies on a three layers model. The results indicated a higher maximum residual stress for the line scanning pattern. Interestingly here, although Cheng et al. (2016) have verified a wide range of scan track, all the considered paths happened to be either continuous with no laser interruption or, in the case of the island scanning, a lump of continuous tracks. This idea will represent the insight of

our proposed research.

In order to better understand the origin residual stress, Mercelis and Kruth (2006) developed a simple theoretical model and conducted several experimental trials with stainless steel powder to measure the stress level. It was found that residual stress was mainly affected by the scan strategy along with the material property and substrate height. Based on a FE analysis, Dai and Shaw (2002) investigated the effect of laser scanning patterns on residual thermal stresses and distortion. They stated that the laser pattern that changed its direction normally (90^o) at every turn was able to reduce the distortion to one third compared to the standard scan strategy.

This short literature review has clearly demonstrated that the quality and mechanical properties of the finished part, in terms of residual stress level, are mainly influenced not only by the selection on the laser parameters (speed/power) but also by the applied scanning strategy as well. Therefore, this study focussed on the development and the validation of a novel scanning strategy that reduces the distortion and residual stresses by lowering the concentration of heat over the course of the build-up process. For this, a three-dimensional thermo-mechanical FE model was developed to predict the temperature history as well as the residual stresses on the work piece. This was achieved by considering temperature dependent material properties and the element “birth and death” technique on a multilayer build. The following sections present in details the model used to simulate the build-up; the validation against experimental data and numerical simulations found in the literature. Finally, the residual stress and deformation, obtained from the new scan strategy studied that considers a novel intermittent laser path in order to avoid heat concentration and reduce the residual stress are presented.

2. Modelling definition

This work considers a thermo-mechanical one-way coupled approach, where the heat generated by mechanical deformation is neglected Denlinger et al. (2014), and an elastoplatic temperature dependent material. The temperature field is computed by solving first the transient heat transfer problem (ie: thermal analysis),

and transferring the computed temperature field to the mechanical analysis at each time-step level. Furthermore, the load force provided by the temperature field is applied through the thermal expansion coefficient of the material, whilst the birth and death strategy is considered to simulate the build-up by activating the element when certain criteria are reached.

2.1. Thermal analysis

The heat conduction in a body with isotropic material is defined by the energy equation:

$$\rho C_p \left(\frac{\partial T}{\partial t} + \boldsymbol{u} \cdot \nabla T\right) = -\nabla \cdot \boldsymbol{q} + Q \quad (1)$$

where ρ is the density, $C_p$is the specific heat capacity, $\boldsymbol{q}$ is the heat flux, T is the temperature, $\boldsymbol{u}$ is the speed and Q is the rate of heat per unit of volume.

Considering there is no motion of material, $\boldsymbol{u}$ is neglected leading to a quasi-steady state problem. Therefore, the energy balance equation can be written as:

$$\frac{\partial H}{\partial t} = -\nabla \cdot \boldsymbol{q} + Q, \text{ in } \Gamma \quad (2)$$

where H is the enthalpy, defined as:

$$H = \int \rho C_p dT \quad (3)$$

Thus, the distribution of heat through the part is given by the Fourier's conduction equation:

$$\boldsymbol{q} = -k\nabla T \quad (4)$$

where k is the thermal conductivity.

For the particular case of an SLM process, additional terms such as initial and boundary conditions should be incorporated in order to reproduce the particular loads, as shown in Figure 1. The preheating of the substrate is expressed as:

$$T = T_0 \text{ at } t = 0, \text{ in } \Gamma \quad (5)$$

where T_0 is the ambient temperature, Γ being the whole domain

The heat flux input accounts as the laser beam:

$$\bar{q} = (-k\nabla T)\,\vec{n}, \text{ on } \Gamma_q \quad (6)$$

where Γ_q is the boundary where the laser heat flux is applied, $\vec{n}$ is the unit normal vector to the surface and $\bar{q}$ is the laser heat flux applied on the boundary.

The Newton's law of cooling accounts as the heat loss through convection:

$$q_{conv} = (-k\nabla T)\vec{n} = h(T_S - T_0), \text{ on } \Gamma_{\text{conv}} \quad (7)$$

where h is the film convection coefficient of the domain, Γ_{conv} is the boundary where convection is applied and T_S is the temperature on the surface. Heat loss through thermal radiation and material vaporisation are neglected, as being beyond of the scope of this work.

2.2. Mechanical analysis

The structural analysis assumed a small strain and displacement formulation in order to obtain the stress and deformation of the work piece during deposition. Once the thermal equation was solved, the temperature field at each time step was applied as body force to the structural component. The governing stress equilibrium equation is described as:

$$\nabla\boldsymbol{\sigma} + \boldsymbol{b} = \mathbf{0} \quad (8)$$

where $\boldsymbol{\sigma}$ is the Cauchy stress tensor and $\boldsymbol{b}$ is the body force. The constitutive relation can be expressed as:

$$\boldsymbol{\sigma} = \boldsymbol{C}\boldsymbol{\epsilon}^e \quad (9)$$

$$\boldsymbol{\epsilon} = \boldsymbol{\epsilon}^e + \boldsymbol{\epsilon}^{\boldsymbol{p}} + \boldsymbol{\epsilon}^T \quad (10)$$

where $\boldsymbol{C}$ is stress-strain matrix and $\boldsymbol{\epsilon}$, $\boldsymbol{\epsilon}^e$, $\boldsymbol{\epsilon}^p$ and $\boldsymbol{\epsilon}^T$ is the total strain, elastic strain, the plastic strain and the thermal strains, respectively. The thermal strain can be calculated as:

$$\boldsymbol{\epsilon}^T = \alpha\big(T - T_{ref}\big)\mathbf{I} \quad (11)$$

where α is the coefficient of thermal expansion, T_{ref} is reference temperature and $\mathbf{I}$ is identity matrix.

The von Mises yield criterion and Prandtl-Reuss flow rule are applied to determine the plastic strain:

$$f = \sigma_m - \sigma_y(\boldsymbol{\epsilon}^{\boldsymbol{p}}, T) \quad (12)$$

$$d\boldsymbol{\epsilon}^p = d\boldsymbol{\lambda}\frac{\partial f}{\partial \boldsymbol{\sigma}} \quad (13)$$

where f is the yield function, σ_m is Mises' stress, σ_y is the yield stress, $d\boldsymbol{\epsilon}^p$ plastic strain increment and $d\boldsymbol{\lambda}$ is the plastic multiplier**.** More details on the formulation of the thermomechanical analysis are described in Bathe (1996).

2.1. Element birth and death

Here, the “element birth and death” technique was adopted in order to mimic the deposition of added material layers during the process. As required by the FE methodology, the work-piece design space needs to be initially fully meshed by creating all the finite elements in the model to compute its full stiffness matrix. The SLM process starts by deactivating the elements that are not yet scanned by nullifying (ie: multiplying by a small number) their contribution to the global stiffness matrix. At the time those elements are activated, the stiffness matrices return to the original value. In the thermal model, when analysis starts all elements of the first layer are activated as a powder material. The material property of the element is changed from powder to solid material when the element has any node that reaches the melt temperature. As the laser scans the entire layer, the elements that belong to the next layer are activated as powder material and the procedure is repeated.

Similarly, for the mechanical model, all elements belonging to the part are deactivated, as the powder has no meaningful mechanical property (no stiffness contributions from the powder). On the other hand, they return to their original state when they have any node that exceeds the melt temperature. The flow chart of FE model is shown in Figure 2.

2.2. Laser modelling

In the SLM process, the laser is activated and heats the powder material, and then an energy transfer occurs. Those physical processes can be divided basically in three categories: energy absorption, heat dissipation and phase transformation.

Part of the energy generated by the laser is absorbed by the powder material, increasing the material temperature beyond the melting point, whilst the remainder is dissipated through conduction to the powder material or convected from the powder bed to the air in the chamber. On the other hand, the powder bed is not able to absorb all the energy and a fraction end up being reflected.

In order to better simulate the laser beam power delivery to the build within the SLM process, many moving heat source model have been developed. The simplest models assume a point source, which is not close to reality. Moreover,

Roberts et al. (2009) used a two-dimensional Gaussian profile function to define the beam. The most commonly applied heat flux model assumes a Gaussian function such as:

$$\overline{q} = \frac{A\,P}{\pi R^2} e^{-B\left(\frac{r}{R}\right)^2} \quad (14)$$

where $\overline{q}$ is the heat flux of Gaussian model, A is the absorptance, P is the laser power, R is the laser spot radius, B is the shape factor and r is the distance to the laser beam centre. Inspired by this equation, Patil and Yadava (2007), Hussein et al. (2013b) and Dong et al. (2009) employed different laser beam shape aiming to simulate laser melting with distinctive features. In this work the Gaussian distribution with the shape factor equal to 2 is adopted as shown in Table 1.

3. Results

In order to validate the proposed numerical approach, three stages have been adopted: (1) a comparison of thermomechanical model against published experimental trials was presented. This was followed by (2) an assessment of three laser scans strategies showing the contrast between the final displacements of each strategy. Finally (3), the proposed novel scanning strategy sequence was introduced to alleviate the concentration of heat by altering the laser path. All considered strategies are intermittent, which means the laser is able to switch on and off in order to dissipate the heat. Findings were then contrasted against traditional scan strategies, showing the displacement of the substrate after total cooling down.

3.1. Validation of thermal analysis with experiment

In order to validate our approach, our thermal model finding were contrasted against the experimental work of Kolossov et al. (2004) and the numerical results obtained by Kundakcioglu et al. (2016) and Huang et al. (2016). Kolossov et al. (2004) conducted an experiment on a 5x5x2 mm titanium powder with 2 mm of layer thickness on a steel substrate without preheating. The laser scanned a 2x2 mm area in the c entre of the domain, measuring the temperature on half of the second scan vector, at point coordinates X=1.85 and Y=2.5. The process parameter used in the

experiment is shown in the Table 2 where the material powder was considered to have absorbed the entire heat flux.

This work applied the same boundary conditions and solid material properties suggested by Kolossov and his colleagues. However, other common approach was adopted for the thermal conductivity of the powder material. It was assumed a constant value of 0.2 W/mK for temperatures below the sintering temperature (1300 ^{o}C) and increasing linearly reaching the correspondent value at the melt temperature (1650 ^{o}C), as presented in Figure 3. This approach emulates the phase transition from powder to liquid. Furthermore, as soon as the temperature exceeded the melt temperature those elements with any node with a temperature greater than melt temperature had their material property switched from powder to bulk material. The thermal model predicted a maximum temperature of 2440 ^{o}C, whereas the measured was 2400 $\pm$ 200 ^{o}C. Figure 4 shows the temperature profile of the experimental and numerical solution of the thermal problem along the X-axis and Y-axis.

The trend presented methodology is in good agreement with the experimental data in contrast to the other numerical techniques of Kundakcioglu et al. (2016) and Huang et al., (2016). The proposed technique was not only able to accurately predict the melt pool temperature and shape, but the temperature on the scanned material as well, which is vital to the SLM process. Moreover, the modelling of thermal conductivity, especially the transition from power to bulk material, was found to be crucial for an accurate temperature prediction around the area of laser application and the rest of the powder bed.

3.2. Validation of mechanical analysis with experiment

A set of experiments carried out by Cao et al. (2016) was selected to validate the residual stress and deformation of the proposed mechanical model. In this experiment a 250x12x2 mm wall was built on a 300x100x14 mm substrate with Ti-6Al-4V material using Direct Energy Deposition technology, for which the process parameters are described in Table3. By adopting the same process conditions of the

experiment and matching the material properties, the simulation predicted that an accurate solution would be found when preheating the substrate to 200 ^{o}C. Here, a 3D Gaussian heat flux distribution was found to better represent the temperature distribution for such a process, agreeing with Goldak et al. (1984).

The computed deformation and Von-Mises residual stress along the centre line on the bottom of the substrate was in good trend agreement with Cao et al. (2016) experimental work as illustrated in Figure 5 and 6. The minimum displacement of the numerical model in Figure 5 reached 225 mm while the experimental result indicated 230 mm, a difference of 2.22%. In Figure 6, with an experiment uncertainty of 50 MPa, the numerical results in the center of the part reached 272.0 MPa while the experimental outcome was 292.6 $\pm$ 50 MPa. The simulated result was obtained after cooling down the whole geometry to the ambient temperature of 20 ^{o}C and releasing the support adopted over the course of the simulation.

The successful validation of the thermomechanical model provided confidence to apply the developed computational technique to other additional applications involving additive manufacturing study. In the following section, a six scan paths and a proposed methodology to define the laser scan strategy capable of reducing the residual stress on the component is introduced.

3.3. Residual stress reduction and path redefinition

This time and in order to investigate the effect of the scanning strategy on the residual stress and deformation, five different paths were introduced: two conventional paths, commonly used in most build-up processes; two paths with half of the scan vector of the conventional paths but with a distinctive scan sequence and the last strategy with the shortest random scan vector – a novel strategy for such a process. Furthermore, the deformation of the substrate during a single layer powder bed scanning was used as a means to evaluate the effect of the laser path on both the resultant deformation and the residual stress.

3.3.1. Model description

The domain of thermal elastoplastic analyses consisted of a Ti-Al6-V4 powder bed of 1 x 1 mm with a single thick layer of 0.05 mm built on the centre of a Ti-Al6-V4 solid substrate of 3 x 3 x 1 mm using uniform 0.025 mm 8 noded hexahedral elements. Both the width of the hatched region and the melt pool were 0.1 mm, giving a total of 10 tracks per layer, as shown in Figure 7. The whole domain had an ambient temperature of 20 ^{o}C and the computation considered a total of 200 time steps per layer. In addition, the birth/death strategy was used to simulate the deposition of successive layers. Over the course of the build the bottom of the base plate was maintained fixed until the component was cooled to the room temperature, then the based was freed except for the four extremity nodes of the bottom face of the substrate which remained fixed in order to allow for the deformation to take place whilst avoiding the numerical difficulty of rigid body motion. The deformation along the lines AB and CD, at the final stage, was used to measure the amount of distortion generated by the build-up.

In this section, three different laser paths were considered: two conventional paths, unidirectional (Figure 8a) and zigzag (meander/S-shape – Figure 8b), used in most manufacturing processes and a third path consisted of an unidirectional scanning strategy in odd then even vectors sequence in order to reduce the heat concentration, as shown in Figure 8c.

The temperature dependent thermal properties of solid and liquid Ti-Al6-V4 considered for the part and the substrate, were taken from experiments executed by Mills (2002) and Boivineau et al. (2006), and depicted in Table 4. Furthermore, the powder material properties, listed in Table 5, was taken from experimental test performed by Parry et al. (2016).

A comparison of temperature field revealed that the size and shape of the melt pool were the same for all simulated scan strategies (ie: width of 0.1 mm and length of 0.15 mm, a 3D view of the melt pool is illustrated in Figure 9). Also, an asymmetric melt pool was observed due to the interplay of multiple material phases during the simulation. As previously consolidated areas turn into solid material, with a higher conductivity than the surrounding powder material, the heat tended to flow

preferentially through those regions which results in distorting the melt pool. However, in the alternating path, even though the temperature field was not symmetrically distributed throughout the plate due to the scan sequence, the heat was more dispersed throughout the part, as shown in Figure 10. Subsequently, the result was a symmetric deformation, while the unidirectional and zigzag scans were slightly deformed on the side where the powder was first consolidated, as illustrated in Figure 11 and 12. Moreover, as a result of the process of the unidirectional and zigzag scans, the residual stress deformed the base plate after being cooled to room temperature and supports released. Thus, the unidirectional scan deformation was found to be -4.17 μm, while the zigzag -3.75 μm. And interestingly, for the alternating strategy, the distortion was -3.40 μm, revealing a reduction of 18.4% in contrast to the unidirectional and 9.3% in contrast to zigzag. Furthermore, the residual stress distribution on the consolidated material followed a similar trend to those obtained in Parry et al. (2016) and Denlinger et al. (2017), a lower stress was created near the start and end of the scan vector, while in the centre of the part a great residual stress was generated. Experiments with twin cantilever carried out by Setien et al. (2018) also indicated that the strain in the longitudinal direction being significantly greater than the transversal direction, as shown in Figure 11.

3.3.2. Intermittent laser path definition

As residual stress is mainly caused by a high temperature gradient, a scan strategy was developed dividing the geometry into small islands and scanning them in a pre-selected order to reduce the heat accumulation by avoiding adjacent islands to be scanned consecutively. Therefore, and from the observations above, a novel scanning methodology was developed and where the following island was selected according to:

$$f^j = \alpha_1 d_1^j + \alpha_2 d_2^j, \exists\, R_i \leq d_1^j \leq R_e \quad (15)$$

where f^j was the value assigned to each j island, which was set to zero for those that were not candidate island, and used to determine the next island to be scanned; d_1^j and d_2^j were the distances between the candidate islands and current scanned island and previous one respectively; α_1 and α_2 were weighting factors. Those

factors influenced the selection of the next island. By increasing the ratio α_1/α_2, led to prioritising the selection of the island that was furthest away from the previous scanned island but in the area determined by R_i and R_e. In this work, the weighted parameters were set to $\alpha_1 = 10$ and $\alpha_2 = 1$; R_i and R_e were the distances that limit the islands candidates, as shown in Figure 13. The next island to be scanned was the one with the greatest value of f. When all island candidates have already been scanned, an iterative process started by increasing and decreasing gradually R_e and R_i, respectively, until another island, which has not been scanned yet, was found. This sequence ensured that the following scan island was not neighbouring the two previous islands, spreading the heat throughout the region. Consequently, a lower gradient temperature and deformation were expected. A script was developed in order to implement the scan strategies.

3.3.3. Thermal and mechanical analysis of different paths in a single layer model

Three scan strategies were selected to investigate the effect of the laser path and vector length on the deformation and residual stress in the part. A representation of the scanning sequence is shown in Figure 14 where the scanned area was divided in 10 x 10, creating a total of 100 islands. Each island was heated following a sequence according to its colour. All three strategies used in this example are described in Table 7. The alternating sequence of Figure 14 (a), already introduced before in Figure 12 (c), was considered here to contrast other scan strategies. The paths shown in Figure 14 (b) and (c), with 1.0 mm and 0.1 mm, were defined by using the intermittent sequence, which the parameters R_e and R_i were assumed to be 0.3 and 0.2, respectively.

A comparison of the temperature field at a selected time of 0.106s showed a more uniform temperature distribution throughout the powder surface for alternating as seen in Figure 15 (b) and Figure 15 (c). Although the alternating strategy aimed to increase the heat distribution, this strategy failed to pre-heat the non-consolidated powder material. On the contrary, the proposed intermittent strategy, regardless of the vector length, melted the powder and increased the

temperature in the surrounding powder. A similar behaviour was obtained when the chamber was pre-heated before starting the build-up process, which allowed the reduction the temperature gradient and subsequently the residual stress.

The deflection at the bottom of the substrate after the part cooled down to room temperature and along the lines AB and CD are presented in Figure 16. The Intermittent strategy, based on a 0.1mm scan vector length (case (c)), was able to significantly reduce the deformation by up to 29.7%, leading to a minimum displacement of -3.05 μm, when compared to the -3.40 μm of the alternating strategy. A greater scan vector allowed reducing the deformation in 10.2%, or -2.39 μm. Also, a shorter melt pool was formed with a shorter scan vector length, leading to a more symmetric deflection on the substrate as illustrated in Figure 17. Moreover, this investigation also shows in the Figure 18 that the greater the scan vector length, the greater the residual stress, as reported by Parry et al. (2016) and Gibson et al. (2010). Therefore, the scan strategy played an important role in the built-in residual stress, and when choosing the scan strategy the scan vector length should be minimised. This was the main strategy developed in this research.

In order to evaluate the quality of the manufactured component, further studies are necessary to evaluate the mechanical properties, porosity and surface roughness based on the proposed scan strategy.

4. Conclusion

In this study, a one way coupled thermo-mechanical computational model incorporating a surface Gaussian heat flux was developed and validated against published work. The proposed model was then applied to an ALM procedure to investigate five different scan strategies (unidirectional, zigzag, alternating and Intermittent for 1 and 0.1 mm of vector length) aiming at reducing the residual stress on built components. Here, a single layer Ti-6Al-4V powder and solid temperature dependent material properties were incorporated into the model to study the effect of temperature history, vector length and laser scanning sequence, on residual stress and deformation. Specific conclusions can be drawn from this research as follows:

- A simple change of scanning non-adjacent scan vectors, as showed in the alternating strategy, was able to reduce the deformation.
- As shown in previous numerical and experimental studies and confirmed in this work, the scan strategy influences deformation and residual stress of the component.
- Shorter scan vector length tends to produce lower residual stress and significant changes on the deformation were observed. Moreover, the definition of a sequence for the scan vectors proved to be the most efficient approach to reduce the part deformation.
- For the same scan vector length, the proposed scan strategy was able to lower by about 10% the maximum deformation in contrast to the alternating strategy.
- When combining a lower vector length and the proposed strategy that reduce the heat concentration, a substantial reduction of 42% on the deformation was observed, when compared to the unidirectional strategy.

Further studies will be needed to investigate the effect of the proposed strategy on the quality of the manufactured part, such as part porosity, surface roughness and material strength.

ACKNOWLEDGMENT

The first author acknowledges the financial support provided by Conselho Nacional de Desenvolvimento Científico e Tecnológico – CNPq.

FUNDING

Conselho Nacional de Desenvolvimento Científico e Tecnológico – CNPq.

References

Bathe, K.J., 1996. Finite Element Procedures, Englewood Cliffs New Jersey. Prentice Hall.

Boivineau, M., Cagran, C., Doytier, D., Eyraud, V., Nadal, M.H., Wilthan, B., Pottlacher, G., 2006. Thermophysical properties of solid and liquid Ti-6Al-4V (TA6V) alloy. Int. J. Thermophys. 27, 507–529. https://doi.org/10.1007/s10765-005-0001-6

Cao, J., Gharghouri, M.A., Nash, P., 2016. Finite-element analysis and experimental validation of thermal residual stress and distortion in electron beam additive manufactured Ti-6Al-4V build plates. J. Mater. Process. Technol. 237, 409–419. https://doi.org/10.1016/j.jmatprotec.2016.06.032

Cheng, B., Shrestha, S., Chou, K., 2016. Stress and deformation evaluations of scanning strategy effect in selective laser melting. Addit. Manuf. 12, 240–251. https://doi.org/10.1016/j.addma.2016.05.007

Dai, K., Shaw, L., 2002. Distortion minimization of laser-processed components through control of laser scanning patterns. Rapid Prototyp. J. 8, 270–276. https://doi.org/10.1108/13552540210451732

Denlinger, E.R., Gouge, M., Irwin, J., Michaleris, P., 2017. Thermomechanical model development and in situ experimental validation of the Laser Powder-Bed Fusion process. Addit. Manuf. 16, 73–80. https://doi.org/10.1016/j.addma.2017.05.001

Denlinger, E.R., Heigel, J.C., Michaleris, P., Palmer, T. a., 2015. Effect of inter-layer dwell time on distortion and residual stress in additive manufacturing of titanium and nickel alloys. J. Mater. Process. Technol. 215, 123–131. https://doi.org/10.1016/j.jmatprotec.2014.07.030

Denlinger, E.R., Irwin, J., Michaleris, P., 2014. Thermomechanical Modeling of Additive Manufacturing Large Parts. J. Manuf. Sci. Eng. 136, 061007. https://doi.org/10.1115/1.4028669

Dong, L., Makradi, a., Ahzi, S., Remond, Y., 2009. Three-dimensional transient finite element analysis of the selective laser sintering process. J. Mater. Process. Technol. 209, 700–706. https://doi.org/10.1016/j.jmatprotec.2008.02.040

Foroozmehr, A., Badrossamay, M., Foroozmehr, E., Golabi, S., 2016. Finite Element

Simulation of Selective Laser Melting process considering Optical Penetration Depth of laser in powder bed. Mater. Des. 89, 255–263. https://doi.org/10.1016/j.matdes.2015.10.002

Foroozmehr, E., Kovacevic, R., 2010. Effect of path planning on the laser powder deposition process: thermal and structural evaluation. Int. J. Adv. Manuf. Technol. 51, 659–669. https://doi.org/10.1007/s00170-010-2659-6

Fox, P., Sutcliffe, C.J., Louvis, E., Fox, P., Sutcliffe, C.J., 2011. Selective laser melting of aluminium components. J. Mater. Process. Tech. 211, 275–284. https://doi.org/10.1016/j.jmatprotec.2010.09.019

Fu, C.H., Guo, Y.B., 2014. Three-Dimensional Temperature Gradient Mechanism in Selective Laser Melting of Ti-6Al-4V. J. Manuf. Sci. Eng. 136, 061004. https://doi.org/10.1115/1.4028539

Gibson, I., Rosen, D.W., Stucker, B., 2010. Additive Manufacturing Technologies. Springer US, Boston, MA. https://doi.org/10.1007/978-1-4419-1120-9

Goldak, J., Chakravarti, A., Bibby, M., 1984. A new finite element model for welding heat sources. Metall. Trans. B 15, 299–305. https://doi.org/10.1007/BF02667333

Huang, Y., Yang, L.J., Du, X.Z., Yang, Y.P., 2016. Finite element analysis of thermal behavior of metal powder during selective laser melting. Int. J. Therm. Sci. 104, 146–157. https://doi.org/10.1016/j.ijthermalsci.2016.01.007

Hussein, A., Hao, L., Yan, C., Everson, R., 2013a. Finite element simulation of the temperature and stress fields in single layers built without-support in selective laser melting. Mater. Des. 52, 638–647. https://doi.org/10.1016/j.matdes.2013.05.070

Hussein, A., Hao, L., Yan, C., Everson, R., Young, P., 2013b. Advanced lattice support structures for metal additive manufacturing. J. Mater. Process. Technol. 213, 1019–1026. https://doi.org/10.1016/j.jmatprotec.2013.01.020

Kolossov, S., Boillat, E., Glardon, R., Fischer, P., Locher, M., 2004. 3D FE simulation for temperature evolution in the selective laser sintering process. Int. J. Mach. Tools Manuf. 44, 117–123. https://doi.org/10.1016/j.ijmachtools.2003.10.019

Kruth, J.P., Froyen, L., Van Vaerenbergh, J., Mercelis, P., Rombouts, M., Lauwers, B., 2004. Selective laser melting of iron-based powder. J. Mater. Process. Technol.

149, 616–622. https://doi.org/10.1016/j.jmatprotec.2003.11.051

Kundakcioglu, E., Lazoglu, I., Rawal, S., 2016. Transient thermal modeling of laser-based additive manufacturing for 3D freeform structures. Int. J. Adv. Manuf. Technol. 85, 493–501. https://doi.org/10.1007/s00170-015-7932-2

Langelaar, M., 2016. Topology optimization of 3D self-supporting structures for additive manufacturing. Addit. Manuf. 12, 60–70. https://doi.org/10.1016/j.addma.2016.06.010

Ma, L., Bin, H., 2007. Temperature and stress analysis and simulation in fractal scanning-based laser sintering. Int. J. Adv. Manuf. Technol. 34, 898–903. https://doi.org/10.1007/s00170-006-0665-5

Matsumoto, M., Shiomi, M., Osakada, K., Abe, F., 2002. Finite element analysis of single layer forming on metallic powder bed in rapid prototyping by selective laser processing. Int. J. Mach. Tools Manuf. 42, 61–67. https://doi.org/10.1016/S0890-6955(01)00093-1

Mercelis, P., Kruth, J.-P., 2006. Residual stresses in selective laser sintering and selective laser melting. Rapid Prototyp. J. 12, 254–265. https://doi.org/10.1108/13552540610707013

Mills, K.C., 2002. Recommended Values of Thermophysical Properties for Selected Commercial Alloys. Woodhead Publishing, Cambridge.

Parry, L., Ashcroft, I.A., Wildman, R.D., 2016. Understanding the effect of laser scan strategy on residual stress in selective laser melting through thermo-mechanical simulation. Addit. Manuf. 12, 1–15. https://doi.org/10.1016/j.addma.2016.05.014

Patil, R.B., Yadava, V., 2007. Finite element analysis of temperature distribution in single metallic powder layer during metal laser sintering. Int. J. Mach. Tools Manuf. 47, 1069–1080. https://doi.org/10.1016/j.ijmachtools.2006.09.025

Rangaswamy, P., Choo, H., Prime, M.B., Bourke, M.A.M., Larsen, J.M., 2000. High Temperature Stress Assessment in SCS-6/Ti-6Al-4V Composite using Neutron Diffraction and Finite Element Modeling. Int. Conf. Process. Manuf. Adv. Mater. 836.

Roberts, I. a., Wang, C.J., Esterlein, R., Stanford, M., Mynors, D.J., 2009. A three-dimensional finite element analysis of the temperature field during laser

melting of metal powders in additive layer manufacturing. Int. J. Mach. Tools Manuf. 49, 916–923. https://doi.org/10.1016/j.ijmachtools.2009.07.004

Setien, I., Chiumenti, M., van der Veen, S., San Sebastian, M., Garciandía, F., Echeverría, A., 2018. Empirical methodology to determine inherent strains in additive manufacturing. Comput. Math. with Appl. https://doi.org/10.1016/j.camwa.2018.05.015

Wits, W.W., Bruins, R., Terpstra, L., Huls, R.A., Geijselaers, H.J.M., 2016. Single scan vector prediction in selective laser melting. Addit. Manuf. 9, 1–6. https://doi.org/10.1016/j.addma.2015.12.001

Zhao, X., Iyer, A., Promoppatum, P., Yao, S.-C., 2017. Numerical modeling of the thermal behavior and residual stress in the direct metal laser sintering process of titanium alloy products. Addit. Manuf. 14, 126–136. https://doi.org/10.1016/j.addma.2016.10.005

Figure Captions List

Fig. 14 Representation of the scanning sequence (a) Alternating, (b) 1.0 mm of vector length with Intermittent strategy, (c) 0.1 mm of vector length with Intermittent strategy

Fig. 15 Deformation on the base plate along the AB and CD lines for the three different paths, after cool down to ambient temperature and displacement constrains release

Fig. 16 Vertical deformation on the bottom surface of the substrate: (a) Alternating, (b) 1.0 mm of vector length with Intermittent strategy, (c) 0.1 mm of vector length with Intermittent strategy

Fig. 17 Residual stress on the component: (a) Alternating, (b) 1.0 mm of vector length with Intermittent strategy, (c) 0.1 mm of vector length with Intermittent strategy

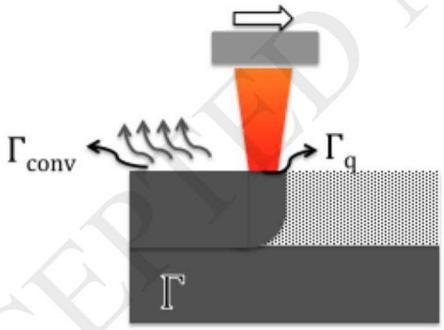

Figure 1 - Schematic representation of SLM heat transfer

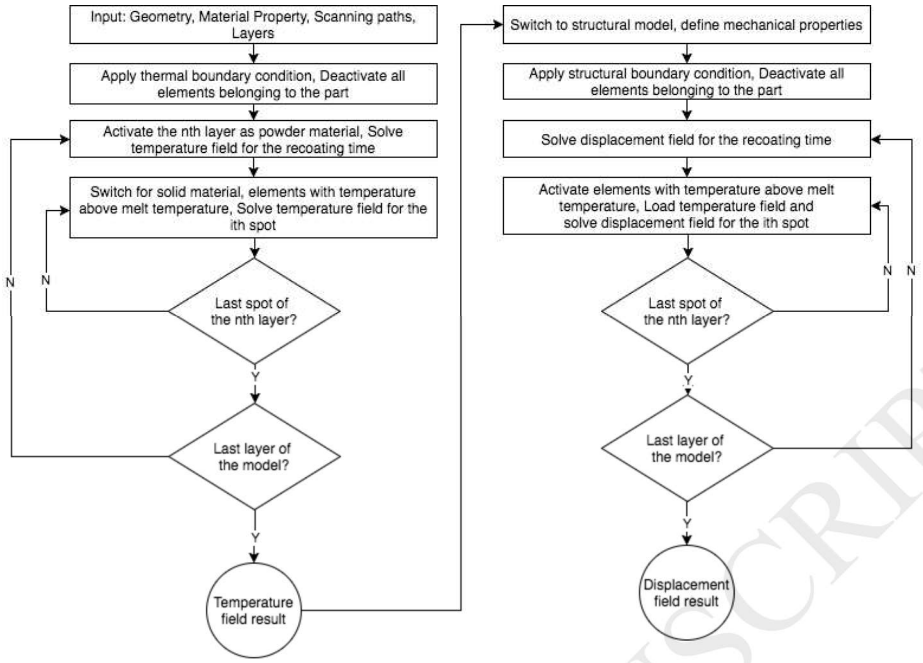

Figure 2 - Flow chart of one-way coupled thermo-mechanical model

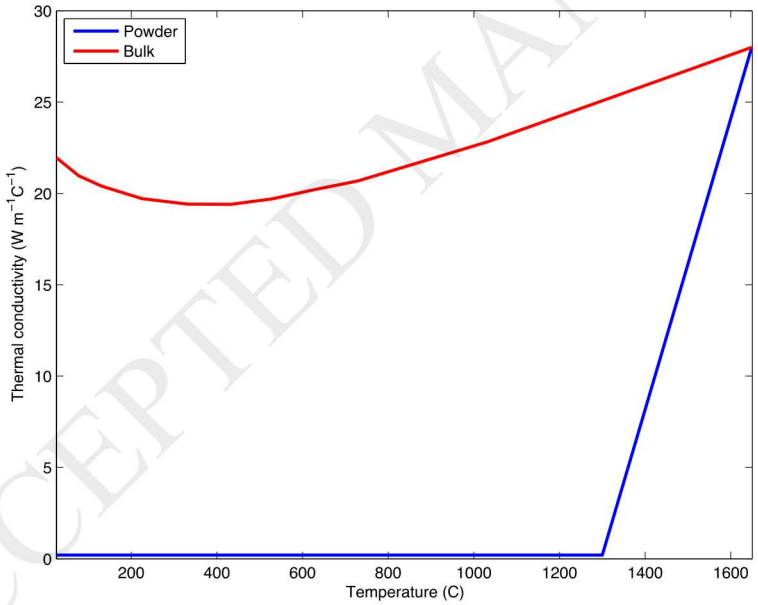

Figure 3 - Thermal conductivity of powder and bulk material

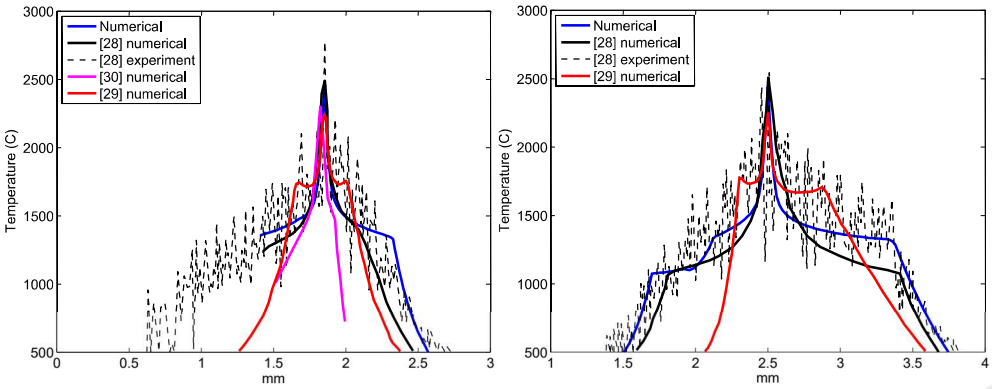

Figure 4 – a) X-Profile of the temperature field at Y=2.5 and Z=2.0 mm; b) Y-Profile of the temperature field at X=1.85 and Z=2.0 mm

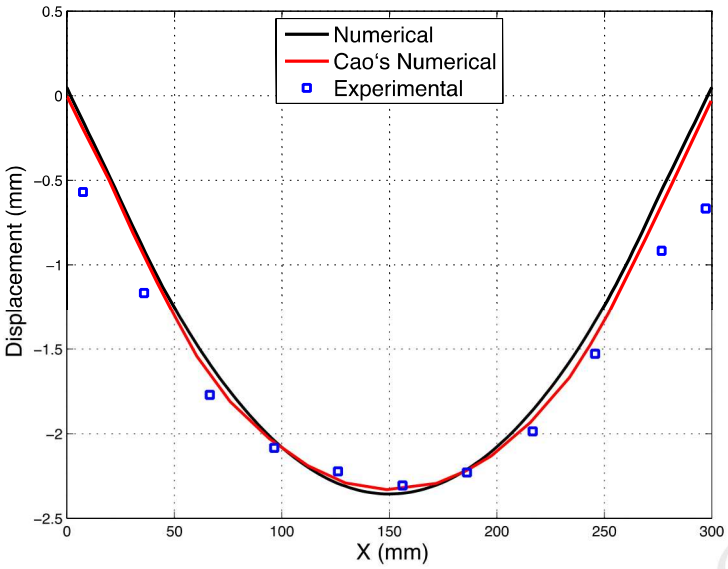

Figure 5 – Vertical displacement along the centre line on the bottom of the substrate

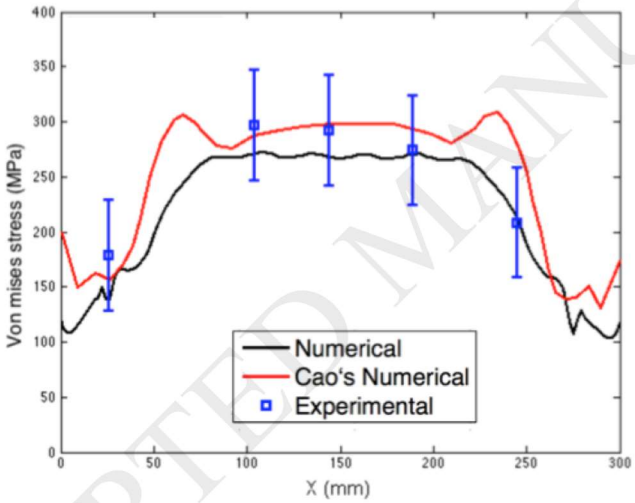

Figure 6 – Von Mises residual stress along the centre line on the bottom of the substrate.

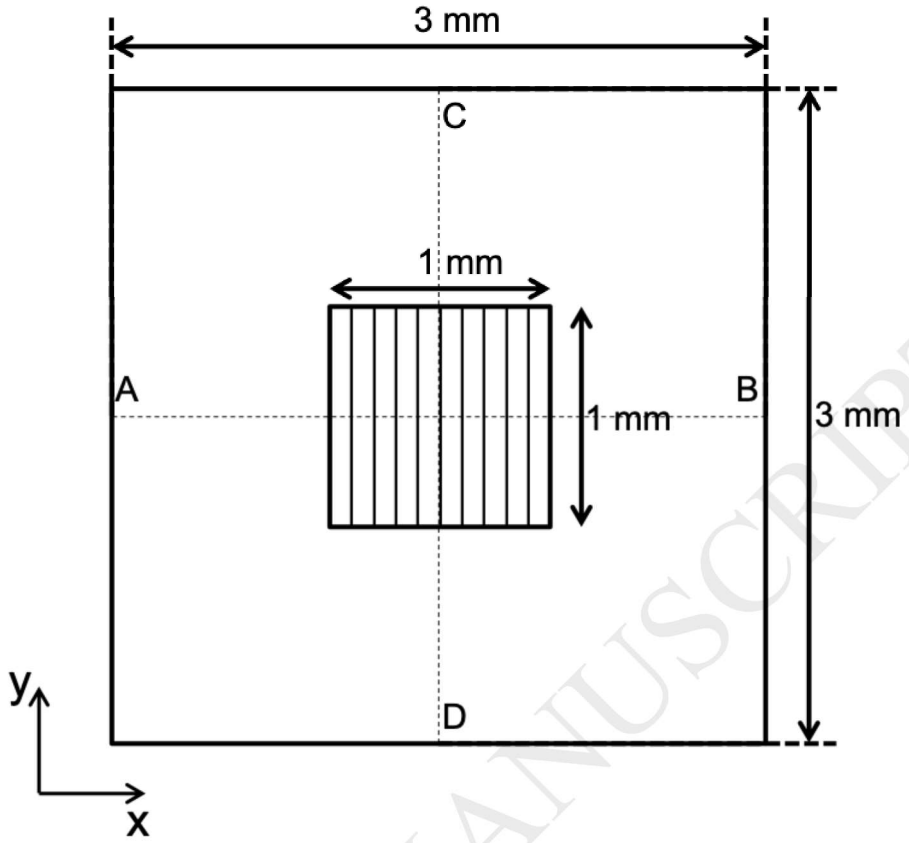

Figure 7 – Model used in the thermomechanical analyses.

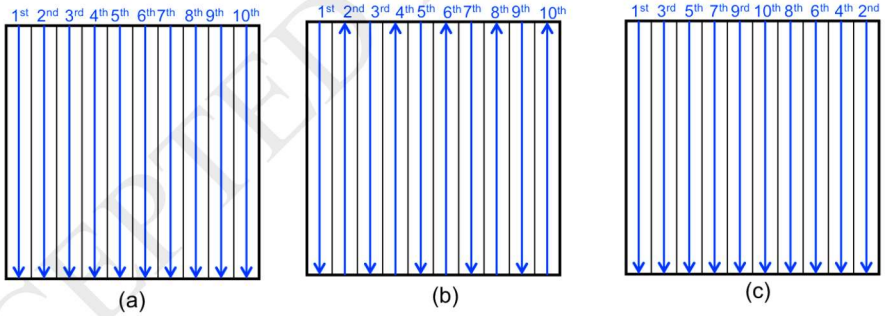

Figure 8 – Laser scan path chosen: (a) Unidirectional, (b) Zigzag and (c) Alternating.

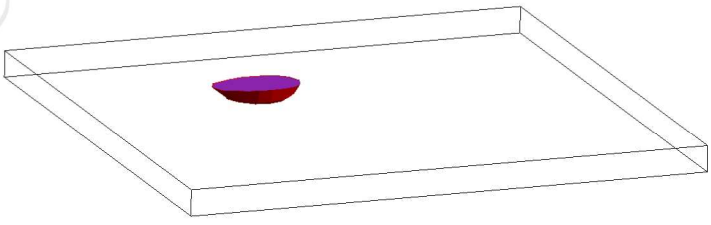

Figure 9 - Melt pool shape during unidirectional simulation.

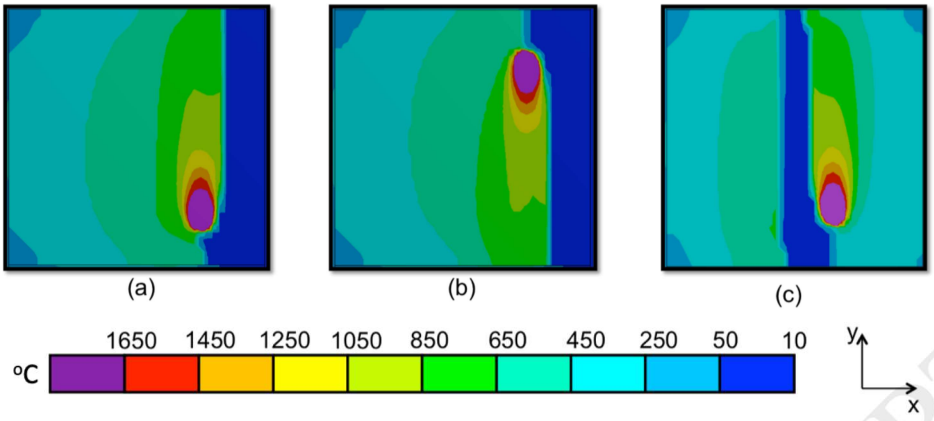

Figure 10 - Temperature field and melt pool at 0.0106 s from a total time of 0.0136 s: (a) Unidirectional, (b) Zigzag and (c) Alternating.

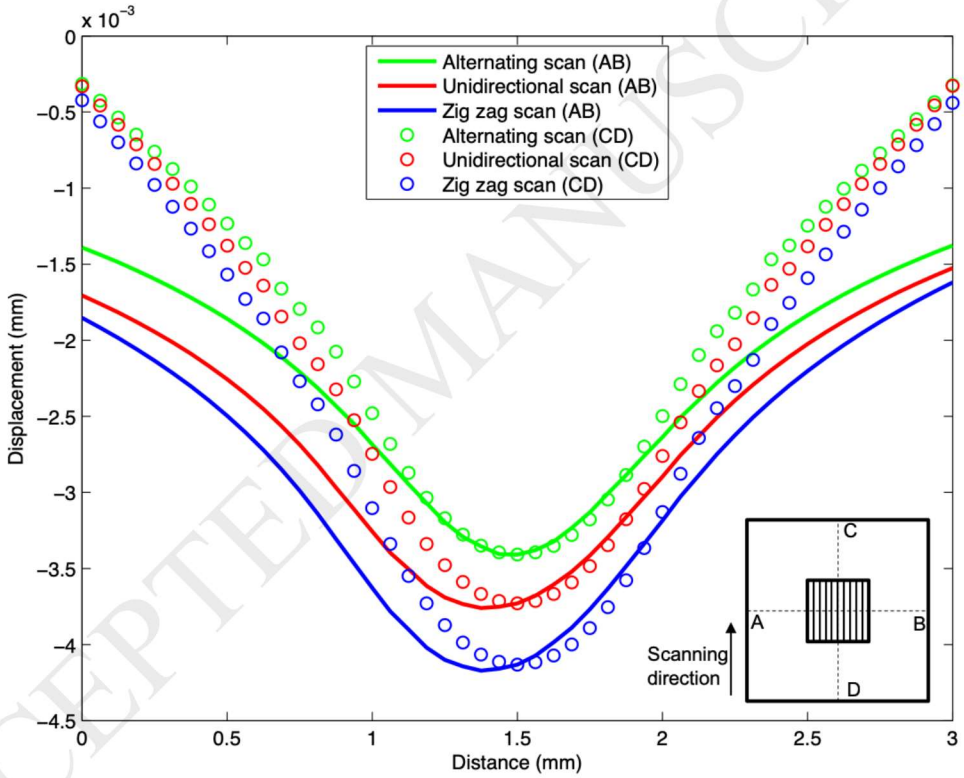

Figure 11 – Deformation on the base plate along the lines AB and CD for the three different paths, after cool down to ambient temperature and displacement constrains release.

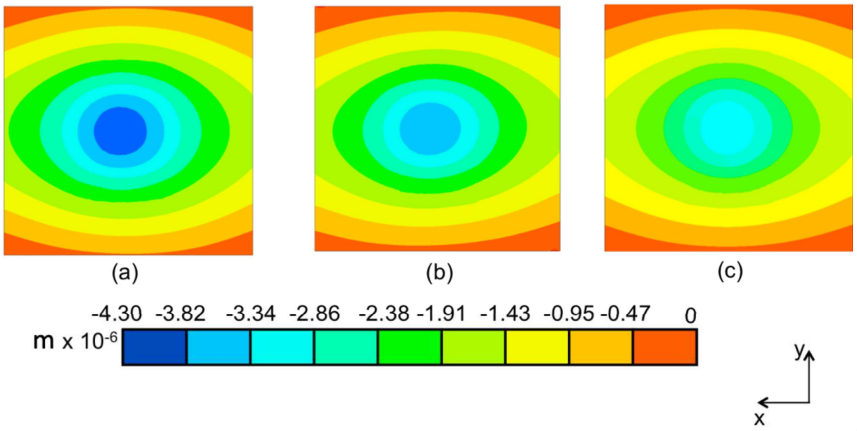

Figure 12 – Vertical deformation on the bottom surface of the substrate: (a) Unidirectional, (b) Zigzag and (c) Alternating.

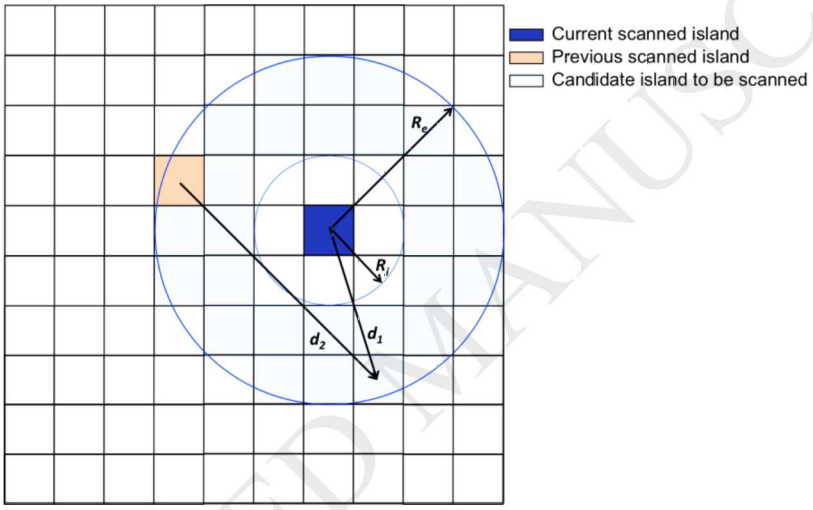

Figure 13 - Islands scanning sequence scheme.

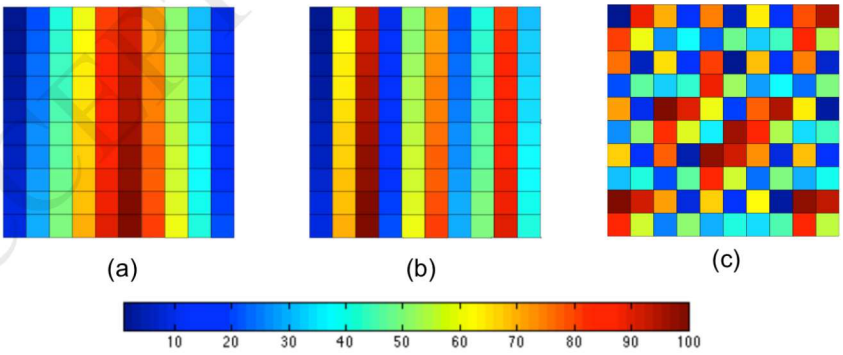

Figure 14 – Representation of the scanning sequence (a) Alternating, (b) 1.0 mm of vector length with Intermittent strategy, (c) 0.1 mm of vector length with Intermittent strategy.

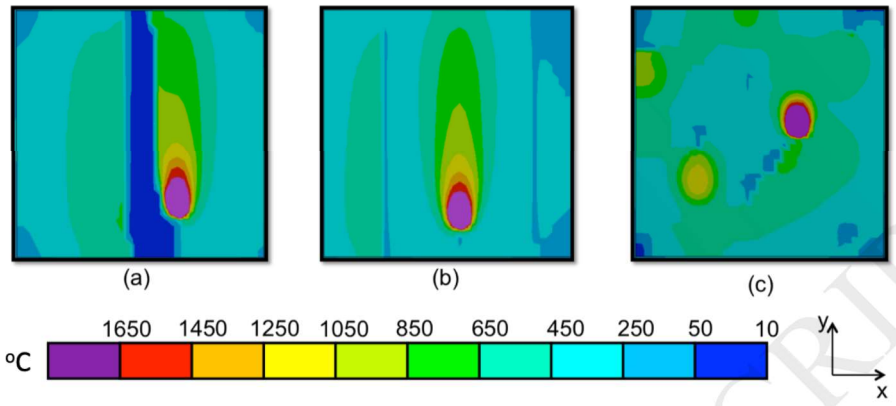

Figure 15 - Temperature field and melt pool at 0.0106 s from a total time of 0.0136 s: (a) Alternating, (b) 1.0 mm of vector length with Intermittent strategy, (c) 0.1 mm of vector length with Intermittent strategy.

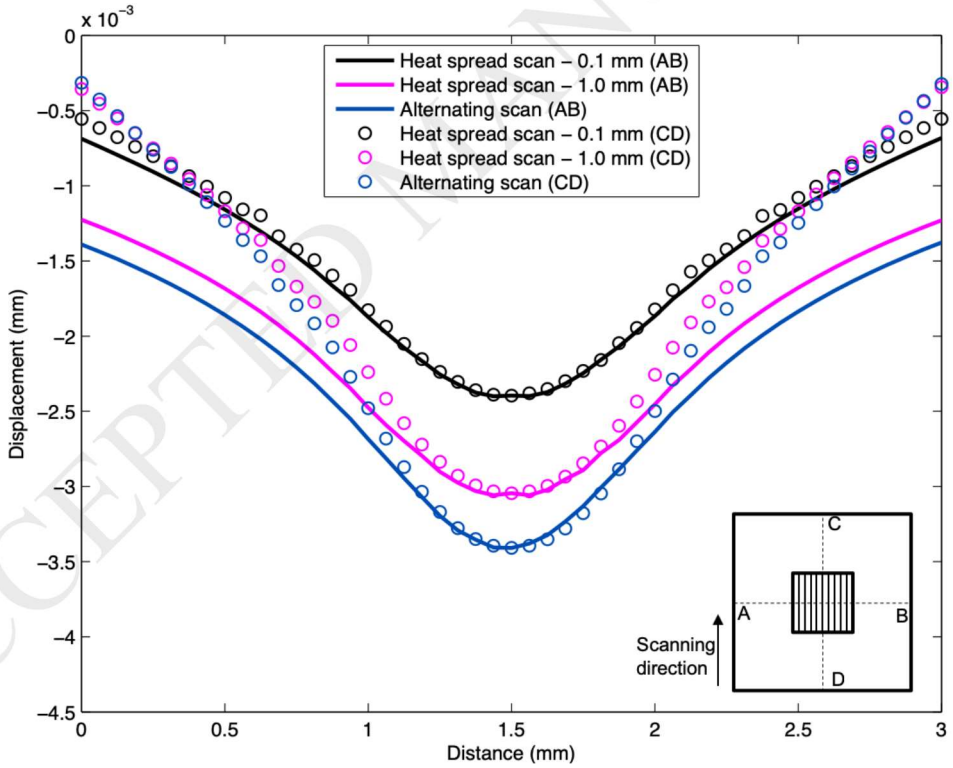

Figure 16 – Deformation on the base plate along the AB and CD lines for the three different paths, after cool down to ambient temperature and displacement constrains release.

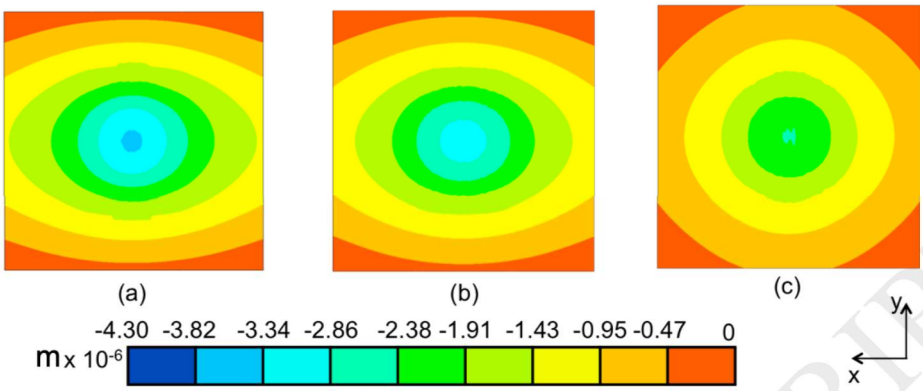

Figure 17 - Vertical deformation on the bottom surface of the substrate: (a) Alternating, (b) 1.0 mm of vector length with Intermittent strategy, (c) 0.1 mm of vector length with Intermittent strategy.

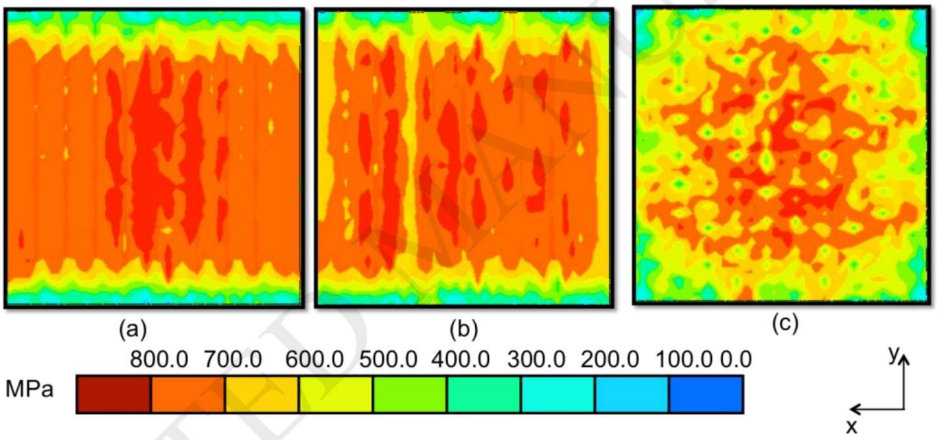

Figure 18 – Residual stress on the component: (a) Alternating, (b) 1.0 mm of vector length with Intermittent strategy, (c) 0.1 mm of vector length with Intermittent strategy.

Table Caption List

Table 1 - Heat flux models

Heat flux type	Heat flux equation	Notes
Surface (2D) heat flux	$Q_{cyl} = \frac{P}{\pi R^2}$	Uniform distribution
	$Q_{G1} = \frac{2AP}{\pi R^2} e^{-\left(\frac{2r^2}{R^2}\right)}$	Gaussian distribution
	$Q_{G2} = \frac{4.55P}{\pi R^2} e^{-4.5\left(\frac{r}{R}\right)^2}$	Alternative shape of Gaussian distribution
Volume (3D) heat flux	$Q_{3D} = \frac{6\sqrt{3}PAf_s}{abc\pi\sqrt{\pi}} e^{-3\left(\frac{x^2}{a^2}+\frac{y^2}{b^2}+\frac{z^2}{c^2}\right)}$	Ellipsoidal Gaussian distribution

Table 2 - Process parameter adopted in [25]

Parameter	Notation	Value	Unit
Power	P	2	[W]
Spot radius	R	25	[μm]
Laser spot speed	V	1	[mm/s]

Table 3 - Process parameter considered in [28]

Parameter	Notation	Value	Unit
Power	P	9600	[W]
Spot radius	R	12.7	[mm]
Laser spot speed	v	12.7	[mm/s]

Table 4 – Parameters used to simulate the selective laser melting process

Parameter	Notation	Value	Unit
Power	P	100	[W]
Spot radius	R	25	[μm]
Laser spot speed	V	800	[mm/s]
Absorptance	A	30%	

Table 5 – Temperature dependent mechanical property for Ti-6A-Al [34]

Temperature	Elastic Moduli (GPa)	Yield Strength (MPa)	Linear Expansivity Coefficient (1/C)	Plastic tangent modulus [MPa]
24	125.0	1000.0	8.78	700
94	110.0	630.0	9.83	2200
205	100.0	630.0	10.00	2200
317	100.0	525.0	10.70	2200
428	80.0	500.0	11.10	1900
539	74.0	446.0	11.20	1900
650	55.0	300.0	11.70	1900
761	27.0	45.0	12.20	2000
872	20.0	25.0	12.30	2000
1094	5.0	5.0	12.40	2000
1650	0.1	0.1	12.50	100

Table 6- Temperature dependent thermal material properties used for bulk Ti-6A-Al.

Temperature	Thermal Conductivity - Ti-6A-Al (W/m K)	
	powder [17]	bulk [30] [31]
20	0,145	7,07
200	0,104	9,28
400	0,083	11,80
600	0,167	14,50
800	0,279	17,40
1000	0,813	22,00
1200	1,09	25,00
1400	-	26,00
1600	-	27,26
1650		28,62